Accelerated Longitudinal Gray/White Matter Contrast Decline in Aging in Lightly Myelinated Cortical Regions

Didac Vidal-Piñeiro,* Kristine B. Walhovd, Andreas B. Storsve, Håkon Grydeland, Darius A. Rohani, and Anders M. Fjell

Research Group for Lifespan Changes in Brain and Cognition, Department of Psychology, University of Oslo, Oslo, Norway

◆ ━━━━━━━━━━━━━━━━━━━━━━━━━━━━━━━━━ ◆

Abstract: Highly myelinated cortical regions seem to develop early and are more robust to age-related decline. By use of different magnetic resonance imaging (MRI) measures such as contrast between T1- and T2-weighted MRI scans (T1w/T2w) it is now possible to assess correlates of myelin content *in vivo*. Further, previous studies indicate that gray/white matter contrast (GWC) become blurred as individuals' age, apparently reflecting age-related changes in myelin structure. Here we address whether longitudinal changes in GWC are dependent on initial myelin content within tissue as defined by baseline T1w/T2w contrast, and hypothesize that lightly myelinated regions undergo more decline longitudinally. A sample of 207 healthy adult participants (range: 20–84 years) was scanned twice (interscan interval: 3.6 years). Results showed widespread longitudinal reductions of GWC throughout the cortical surface, especially in the frontal cortices, mainly driven by intensity decay in the white matter. Annual rate of GWC blurring showed acceleration with age in temporal and medial prefrontal regions. Moreover, the anatomical distribution of increased rate of GWC decline with advancing age was strongly related to baseline levels of intracortical myelin. This study provides a first evidence of accelerated regional GWC blurring with advancing age, relates GWC patterns to cortical myeloarchitectonics and supports the hypothesis of increased age-related vulnerability of lightly myelinated areas. *Hum Brain Mapp 37:3669–3684, 2016.* © 2016 Wiley Periodicals, Inc.

Key words: gray/white matter contrast; lifespan; aging; myelin; T1w/T2w

◆ ━━━━━━━━━━━━━━━━━━━━━━━━━━━━━━━━━ ◆

INTRODUCTION

Myelin is essential to maintain the speed and synchrony of neural networks on which optimal function depends [Haroutunian et al., 2014]. The density, size and orientation of myelinated axons are regionally specific throughout the cortex [Nieuwenhuys, 2013] suggesting that specific profiles of myeloarchitecture relate to particular cortical functions. Histological studies have shown protracted maturation and age alterations of myelin both in humans and primates [Benes et al., 1994; Feldman and Peters, 1998; Marner et al., 2003; Miller et al., 2012; Yakovlev and Lecours, 1967]. Inverse U-shape lifespan trajectories of myelin have been observed, with more protracted development and increased age effects in frontal and temporal areas [Bartzokis et al., 2001; Grydeland et al., 2013b; Salat

et al., 2009; Westlye et al., 2010], which are known to be relatively lightly myelinated [Glasser and Van Essen, 2011].

Several neuroimaging measures have been proposed to partially account for myelin integrity across the cortical mantle. While diffusion techniques, widely used to assess deep white matter (WM) integrity, may measure myelination to some extent [Beaulieu, 2002; Song et al., 2005], signal intensity and contrast based indices such as T1, the ratio of T1-weighted/T2-weighted (T1w/T2w) and T1w signal intensity might be better suited to reflect myelin content across the cortical surfaces [Glasser et al., 2014]. It has been proposed that gray/white matter T1w contrast (GWC) that measures the blurring between gray matter (GM) and WM boundaries (GW/WM) can capture local variations in myelin content. While neurobiological foundations of GWC are still not well understood, structure and density of myelin sheaths [Raz et al., 1990; Salat et al., 2009; Westlye et al., 2009] arise as the main candidate to explain age-related changes in this contrast; however, other suitable biological explanations have also been hypothesized such as increased water content with age [Magnaldi et al., 1993].

Earlier studies have found alterations of GWC in older adults [Davatzikos and Resnick, 2002; Magnaldi et al., 1993] with tissue boundaries being less differentiated as a function of age. By using cortical reconstruction methods [Dale et al., 1999] which greatly improves the delineation of the GM/WM boundary, a handful of cross-sectional studies have further confirmed strong region-specific GWC reductions in aging [Salat et al., 2009; Westlye et al., 2009]. Frontal and, to a lesser extent, temporal and posteromedial areas show the strongest age-related GWC decay that seems to be mainly driven by pronounced declines of T1w signal intensity in the WM tissue [Westlye et al., 2009]. The trajectories of T1w-GM and T1w-WM signal intensity which showed inverted U patterns were also described in cross-sectional lifespan designs [Westlye et al., 2010], interpreted as a reflection of brain myelination. In this context, longitudinal studies promise to be of great help to characterize tissue signal profiles and GWC across the lifespan expanding the existent knowledge as they seem more sensitive to detect changes in decline slope, specially accelerated decline in the oldest participants [Fjell et al., 2009a]. To date, only two studies have explored GWC index longitudinally. Davatzikos and Resnick [2002] found longitudinal reductions in a GWC index using a whole-brain GM value and without surface reconstruction in cognitively normal older adults (scans at year 1, 3 and 5). More recently, Grydeland et al. [2013a] observed widespread reductions of GWC across the cortical mantle in Alzheimer's Disease patients scanned twice (interscan interval ≈ 2 years) but only small increases of contrast in posterior brain areas in the healthy controls.

In this study we explored the longitudinal GWC trajectories of 207 participants spanning the entire adulthood, and tested to what degree these vary as a function of age and regional baseline intracortical myelin content, computed as T1w/T2w ratios that shows relative variation in myelin content [Glasser and Van Essen, 2011]. Similar analyses were additionally done for T1w-WM and T1w-GM signal intensity. Based on results from cross-sectional studies, we expected widespread annual changes of GWC particularly in the prefrontal cortex as well as to a lesser extent in T1w signal intensity for WM and for GM. We hypothesized acceleration of GWC decline as well as of T1w-GM and T1w-WM signal intensity in older adults based on knowledge from myelin mappings [Grydeland et al., 2013a] and T1w signal intensity age-related profiles [Westlye et al., 2010] that should be evident after late fifties. Finally, assuming a link between myelin and GWC, we expected that lightly myelinated regions would be more vulnerable to detrimental effects of age [Bartzokis et al., 2001] and consequently to GWC decline in the old adulthood.

Abbreviations

CSF	Cerebrospinal fluid
CVLT	California Verbal Learning Test II—Alternative Version
FWE	Family-wise error
FWHM	Full-width at half-maximum
GAMM	Generalized additive mixed model
GM	Gray matter
GWC	Gray/white matter contrast
ICC	Intraclass coefficient analyses
MMSE	Mini mental state examination
MPRAGE	Magnetization-prepared rapid gradient echo
MRI	Magnetic resonance imaging
MT	Magnetization transfer
ROI	Region-of-interest
SD	Standard deviation
T1w/T2w	T1-weighted/T2-weighted

MATERIAL AND METHODS

Sample

The longitudinal sample was drawn from the ongoing project Cognition and Plasticity through the Lifespan, run by the Research Group for Lifespan Changes in Brain and Cognition, Department of Psychology, University of Oslo [Fjell et al., 2008; Westlye et al., 2010, 2011]. All procedures were approved by the Regional Committee for Medical and Health Research Ethics, and written informed consent was obtained from all participants. For the first wave of data collection, participants were recruited mainly through newspaper ads. Recruitment for the second wave was by written invitation to the original participants. At both time points (Tp1, Tp2), participants were screened with standardized health interviews. Participants were required to be right handed, fluent Norwegian speakers, and have

TABLE I. Sociodemographics

Age group	n	Females (%)	Years of education (SD)	Mean age (SD)	Interscan interval (SD)
20–29	34	19 (55.9)	15.0 (1.8)	23.9 (2.8)	3.4 (0.3)
30–39	26	19 (73.1)	17.4 (2.5)	34.9 (2.9)	3.4 (0.2)
40–49	29	20 (69.0)	15.3 (2.2)	46.3 (3.1)	3.9 (0.4)
50–59	54	31 (57.4)	15.6 (1.9)	54.8 (2.6)	4.0 (0.3)
60–69	38	22 (57.9)	16.3 (3.7)	64.4 (2.8)	3.2 (0.2)
70–79	19	9 (47.4)	16.6 (2.9)	71.9 (1.8)	3.1 (0.2)
80–85	7	2 (28.6)	16.1 (2.1)	82.1 (1,5)	3.2 (0.2)
All	207	122(58.9)	15.9 (2.6)	50.3 (16.5)	3.6 (0.5)

Main sociodemographic characteristics stratified by age.

normal or corrected to normal vision and hearing. Exclusion criteria were history of injury or disease known to affect brain function, including neurological or psychiatric illness or serious head trauma, being under psychiatric treatment, use of psychoactive drugs known to affect brain functioning, and magnetic resonance imaging (MRI) contraindications. Exclusion criteria did not extend to vascular risk factors, such as hypertension. Participants were required to score ≥26 on the Mini Mental State Examination (MMSE; Folstein et al., 1975), have a Beck Depression Inventory (BDI; Beck 1987) score of ≤16, and score ≥85 on the Wechsler Abbreviated Scale of Intelligence [Wechsler, 1999]. At follow-up, an additional set of inclusion criteria was used: MMSE score of ≥26; MMSE change from Tp1 to Tp2 of <10%; California Verbal Learning Test II—Alternative Version (CVLT II; Delis et al., 2000) immediate delay and long delay T-score of >30; CVLT II immediate delay and long delay change from Tp1 to Tp2 of <60%. At both time points all scans were evaluated by a neuroradiologist and were required to be deemed free of significant injuries or conditions.

Two hundred and eighty-one participants completed Tp1 assessment. For the follow-up study, 42 opted out, 18 could not be located, 3 did not participate due to health reasons, and 3 had MRI contraindications, yielding a total of 66 dropouts (35 females). Eight of the remaining 215 participants failed to meet at least one of the additional inclusion criteria. This resulted in a final sample of 207 participants (122 females) with a mean age of 50.2 years (SD = 16.5) at Tp1 (range: 20–84 years). Mean scan interval was 3.6 years (SD = 0.5, range: 2.7–4.8 years). Main sociodemographic variables are shown in Table I. No significant relationship was found between age, sex and education ($P > 0.1$ for any test; bivariate Pearson's correlation and unpaired t-test as appropriate). Further sample details and description including cognitive performance information can be found in Storsve et al. [2014]. Independent sample t-tests (and a Chi-square test for sex) revealed that the dropout participants had significantly lower full-scale Wechsler Abbreviated Scale of Intelligence scores ($t = 3.8$ [$P = 1.7e^{-4}$]) but comparable BDI, MMSE and CVLT scores as well as similar age and sex ($P < 0.05$ for any test). A missingness analysis was carried out. See Supporting Information for a detailed description of the analysis. Follow-up participants had slightly higher GWC values in the medial orbitofrontal and the rostral anterior cingulate ROIs at time point 1 ($P = 0.01$ and $P = 0.03$, respectively), though none of them survived multiple comparison correction (Supporting Information Table I). The addition of participants that did not complete the follow-up in the models did not significantly modify lifespan trajectories of GWC (Supporting Information Fig. 1).

MRI Acquisition

Imaging data were collected using a 12-channel head coil on a 1.5 T (Siemens Avanto scanner, Siemens Medical Solutions, Germany) at Rikshospitalet, Oslo University Hospital. For each subject and each time point, two MRI T1w structural sequences were acquired, always with the same scanner and sequence although with minor software upgrades. Intraclass Coefficient analyses (ICC) showed a mean between Region-of-Interest (ROI) GWC values measured at both time points of 0.86 (ICC range = 0.77–0.94; see Supporting Information and Supporting Information Table V), minimizing the possibility of systematic biases due to scanner software upgrades. The pulse sequence used for the study was a 160-slice sagittal T1w magnetization-prepared rapid gradient echo (MPRAGE) sequence (TR = 2,400 ms; TE = 3.61 ms; TI = 1,000 ms; flip angle = 8°; matrix = 192 × 192; FOV = 240 mm; voxel size = 1.25 × 1.25 × 1.20 mm). To compute regional baseline cortical myelin content through T1w/T2w maps, a T2w sampling perfection sequence with application-optimized contrasts using different flip angle evolutions was acquired at baseline for each participant (SPACE, TR = 3,390 ms; TE = 388 ms; variable flip angle, bandwidth = 650 Hz/pixel, FOV = 256 mm, voxel size = 1 mm isotropic voxels). The use of a variable flip angle T2w SPACE sequence seems to improve the sensitivity to myelin that likely arises from T1 and magnetization transfer (MT) effects [Glasser et al., 2014]. Matrix dimensions were 204/256 × 256 × 176 where the first dimension differed across participants. The mean anatomical distribution of myelin maps was not substantially affected by this variation (ICC = 0.94–0.97;

Supporting Information and Supporting Information Fig. 2). Myelin maps from 4 subjects were not computed due to T2w acquisition problems. All the other parameters were identical.

MRI Analysis

Structural T1w raw acquisitions were reviewed for quality and automatically corrected for spatial distortion due to gradient nonlinearity [Jovicich et al., 2006] and field inhomogeneity with a method independent of the field estimate on anatomy [Sled et al., 1998]. Importantly, nonparametric nonuniform intensity normalization does not scale tissue classes to normalized distributions. For each participants and each time point, the two consecutively collected MRI images were coregistered, averaged to improve the signal-to-noise ratio, and resampled to isotropic 1 mm voxels. For each time point, GWC and T1w intensity values were later obtained by projecting each participant's cortical surface to the averaged isotropic T1w image. Next, the images were automatically processed cross-sectionally for each time point with the FreeSurfer software (5.1 version; http://surfer.nmr.mgh.harvard.edu/). The automatized processing pipeline that includes removal of non-brain tissue, Talairach transformation, intensity correction, tissue segmentation, cortical surface reconstruction and cortical parcellation is thoroughly described elsewhere [Dale et al., 1999; Fischl et al., 1999a; Fischl and Dale, 2000]. All volumes were visually inspected and minor manual edits were performed on most subjects (>75%) which were generally limited to removal of non-brain tissue included within the cortical boundary. To estimate longitudinal change, the cross-sectionally processed images were subsequently run through the longitudinal stream in FreeSurfer [Reuter et al., 2012]. Here, an unbiased within-subject template volume based on all cross-sectional images was created for each participant, and processing of both time points were then re-run from this subject-specific template. GWC and cortical thickness (CTh) surface maps were resampled, mapped to a common surface, and smoothed using a Gaussian kernel of 15 mm full-width half-maximum (FWHM; Fischl et al., 1999b).

From this stream, we obtained GWC, T1w signal intensity and CTh change values. Annual rate of change, given by: ([Tp2-Tp1]/interscan interval), was selected as the longitudinal measure of interest. Additionally, (ROI) values for each subject and each time point were used in a generalized additive mixed model (GAMM) analysis and its subsequent spaghetti plots. GWC was estimated by calculating the following contrast from the abovementioned T1w images: $(100*[(WM - GW)/(WM + GM)])$. T1w-GM intensity values were taken at a 0.5 projection fraction from the GM/WM boundary (at mid-thickness) while WM were assessed 1 mm below the GM/WM surface for each vertex. GWC values towards 0 indicate less contrast and

thus more blurring of the GM/WM boundary. Separate T1w signal intensities sampled in subjacent WM and in the GM were also obtained as measures of interest. GWC and T1w signal intensity were additionally computed from several other projection distances to study the stability of these measures across sampling distances; absolute distances were sampled every 0.1 mm, between 0.1 to 1.4 mm, while fractions were sampled every 0.05 fraction, between 0.05 and 0.8 fractions. CTh values, used as regressors to control for cortical atrophy, were automatically computed in the FreeSurfer processing pipeline as the distance in mm between GM/WM and pial surfaces [Fischl and Dale, 2000]. Next, annual rate of GWC and T1w tissue signal intensity cortical maps were fed to statistical analysis. In addition a surface-based labelling system, implemented in FreeSurfer [Desikan et al., 2006; Fischl et al., 2004a], was used to divide the cortical surface in 34 well-known ROIs for each hemisphere. Cortical ROI measures were obtained from unsmoothed, untransformed participants' surface and used for further statistical testing.

To further normalize intensities with respect to scanner and sequence related noise which can greatly influence on T1w tissue signal intensity, mean ventricle cerebrospinal fluid (CSF) intensity was computed for each time point and each participant. Lateral ventricles were obtained by an automated segmentation procedure implemented in FreeSurfer [Fischl et al., 2002, 2004b] after eroding all ventricle segments by one voxel to minimize partial volume effects. Tp2 – Tp1 mean CSF intensity difference was computed and included in all models as an additional regressor. CSF intensity change did not significantly differ from 0 and was unrelated to sex and age when introduced into a general linear model (GLM; $P > 0.05$ for any test). Separate CSF intensity for each time point was used for GAMM analysis.

The pipeline followed to compute T1w/T2w myelin content is thoroughly described elsewhere [Grydeland et al., 2013a]. Briefly, raw T1w images were preprocessed cross-sectionally with the previously described FreeSurfer pipeline; T2w maps were linearly registered within-subject to the unresampled T1w image using highly accurate cross-modal boundary-based registration techniques [Greve and Fischl, 2009] and applied using spline interpolation to minimize tissue contamination from CSF and WM signal [Glasser and Van Essen, 2011]. The T1w volume was then divided on the aligned preprocessed T2w volume, creating a T1w/T2w image for each subject. T1w/T2w values were sampled vertex-wise at a distance of 0.2 mm into the GM from the GM/WM boundary [as in Grydeland et al., 2013a] and at mid-thickness (0.5 fraction, as GWC in the present study) yielding T1w/T2w surfaces for each individual. As control, we also sampled T1w/T2w values at 1.0 mm below the cortical surface. Next, the T1w/T2w surfaces were mapped to a common surface, averaged across participants, smoothed at 15 FHWM and fed to statistical analysis with the purpose of assessing the

topological correspondence with GWC estimates. Minor distortions during T2w to T1w registration cannot be completely discarded –which can lead to incomplete cancelation of bias field- nor partial volume effects [Shafee et al., 2015], especially in the occipital cortex and the postcentral gyrus [Grydeland et al., 2013a]. However, the smoothing, and the statistical analysis carried with T1w/T2w maps in the present study, minimizes the effects of partial volume effects on the results.

Statistical Analysis

Statistical analyses were performed by use of FreeSurfer (5.3 version; http://surfer.nmr.mgh.harvard.edu/), MAT-LAB (R2014b; www.mathworks.com/products/matlab) and IBM SPSS 20.0 (Statistical Package for Social Science, IL). Spaghetti plots and longitudinal curve fitting were performed using MMIL Data portal (//mmil-dataportal.ucsd.edu/Bartsch et al., 2014) which uses functions freely available through the statistical environment R (http://www.r-project.org/). When not explicitly specified data refer to mean [standard deviation (SD)].

The longitudinal effects of interest were annual rate of GWC and T1w signal change and its interaction with age (i.e. to assess acceleration or deceleration of GWC and T1w signal change). For each longitudinal measure (GWC, T1w-WM, T1w-GM) and each hemisphere, a series of independent GLMs were calculated with age, sex, CSF intensity change, and per-vertex CTh rate of atrophy as predictors. Family-wise error (FWE) correction method was used to correct for multiple comparisons by thresholding all cortical vertices at $P < 0.01$, and testing surviving clusters against an empirical null distribution of maximum cluster size across 10.000 iterations using Z Monte Carlo simulations [Hagler et al., 2006; Hayasaka and Nichols, 2003] at $P < 0.05$ (two-sided; Bonferroni corrected for bihemispherical comparison [$n = 2$]). All the described voxelwise cortical statistical analyses methods were used as implemented in FreeSurfer.

In addition to the vertex-wise analyses, ROI analyses were performed. Annual rates of GWC, T1w-WM and T1w-GM change were obtained bihemispherically for the 34 cortical ROIs. As no significant hemisphere differences in annualized change were observed for any ROI (two sample t-test; $P < 0.05$; Bonferroni corrected [$n = 34$]), subsequent analyses were done with bilateral ROIs. ROI measures were analysed similarly to voxelwise analysis. For each ROI, GWC and T1w signal rates were introduced in independent GLM models with age, sex, CSF intensity change, and ROI's CTh rate of atrophy as regressors (see Supporting Information Tables II–IV for model estimates with and without CSF intensity change and rate of CTh atrophy as regressors). Grand mean estimates of change (annual change) and estimates and significance of age were the main outcomes of interest. Effect sizes were additionally computed following published guidelines [Lakens,

2013]. The same models were implemented to study the variation of contrast and intensity change at different sampling distances. To further explore adult lifespan trajectories of GWC and T1w signal intensity, ROI measures from each time point were introduced into a GAMM analysis where the predicted variables were GWC and T1w signal intensity, the predictor was age while CSF intensity, sex and CTh were treated as covariates (adjusted prior to GAMM routine through linear mixed effect models). GAMM extends the generalized mixed model by allowing the predictor function to also include a priori unspecified smooth functions of some or all the covariates and can be represented as the following formula: $G(y) = X^*\alpha + \sum_{j=1}^{p} f_j(x_j) + Zb + \epsilon$ where $G(\cdot)$ is a monotonic differentiable link function; α the vector of regression coefficients for the fixed parameters; X^* the fixed effects matrix; f_j the smooth function of the covariate x_j; Z the random effects model matrix; b the vector of random effects coefficients and ϵ the residual error vector [Wood, 2006]. GAMM fitting was showed over its correspondent spaghetti plots. The GAMM technique is a flexible and straightforward tool that maximizes the quality of fitting a dependent variable, especially in presence of nonlinear relationships. The mixed-effects routine allows to model between and within-subject variability as well as time-varying covariates such as CTh and CSF intensity. The main drawback of this technique is overfitting; yet conservative patterns (knots = 5) were chosen to minimize the risk. One young subject was excluded from GAMM analysis as a result of extreme adjusted T1w signal intensity values. Due to space limitations, only a representative set of ROIs, that includes cuneus, entorhinal, rostral anterior cingulate, superior frontal, middle temporal, pars triangularis, postcentral and supramarginal ROIS, are shown in the figures.

To compare the anatomical characteristics of the myelin maps to the GWC and T1w signal longitudinal maps, each type of cortical map was Z-standardized and fed to random subsampling statistical analysis. To avoid collinearity between adjacent voxels, subsets of vertices (2% of all cortical vertices) were randomly selected and, next, bivariate Pearson's correlations between the myelin-estimates and the GWC and T1w signal intensity change were computed within these subsets of vertices. This process was iteratively repeated ($n = 5,000$). Rank-based median from all the iterative correlations obtained in each subsample of vertices were selected as the measures of interest. The analysis was performed independently for each hemisphere.

RESULTS

Annual Rate of GWC And T1w-Tissue Signal Intensity Change in the Cortical Mantle

Whole cortex annual rate of GWC change was −0.06 (0.11), with a yearly reduction of −0.34% (0.69), showing a significant reduction of the contrast at Tp2 ($P < 10^{-12}$;
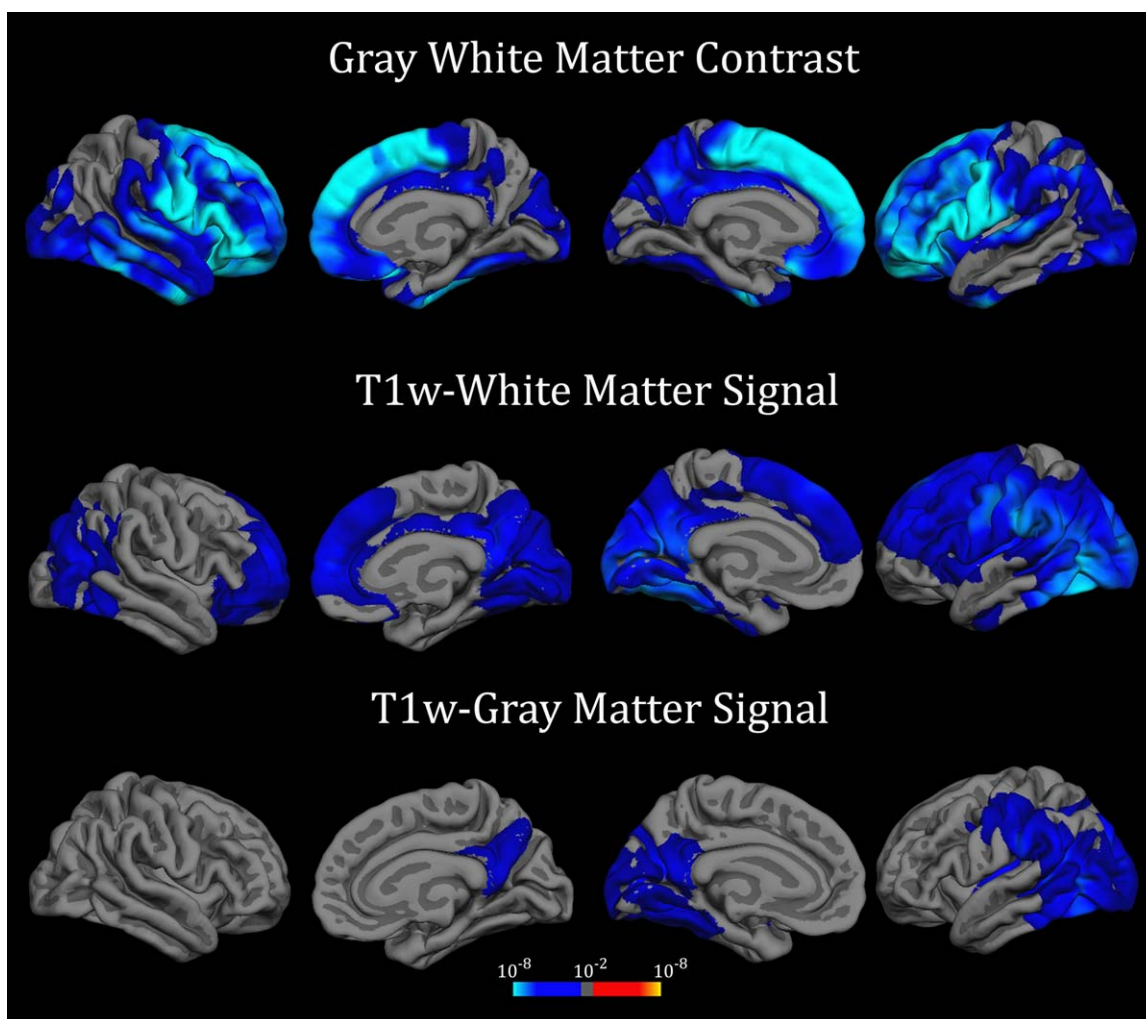
Figure 1.

Annual rate of GWC and tissue signal intensity changes. Annual rate of GWC and tissue signal intensity changes after FWE correction for multiple comparisons. Displayed results are thresholded at P < 0.01 vertex-wise and P < 0.05 cluster-based (Bonferroni corrected). Blue-Lightblue scale indicates GWC or signal intensity longitudinal decline (in P-values).

Cohen's d_z = 0.54). Annual T1w intensity signal change in the WM was −0.45 (1.96) and in the GM was −0.20 (1.44) also exhibiting significant reductions at Tp2 (P = 0.001, d_z = 0.23 for WM and P = 0.04, d_z = 0.14 for GM) and with a yearly reduction of −0.27% (1.29) and −0.15% (1.29), respectively. As shown in Figure 1, after adjusting for sex, CSF intensity change and vertex-dependent annual rate of CTH atrophy, we observed FWE corrected GWC decay in widespread areas of the cortical surface. GWC decrements were more prominent in the superior and inferior frontal cortex but were also highly significant in several portions of the temporal lobe bilaterally. T1w intensity changes were also evident in widespread areas of the superficial WM especially in the posterio-occipital

cortex and in the superior frontal gyrus. To a lesser degree, posterior regions of the brain also showed longitudinal T1w intensity signal decay when sampled into the GM cortex. As no significant hemisphere differences in annualized –GWC and T1w signal intensity- change were observed for any cortical ROI, apparent hemispherical differences in the vertex-wise analyses likely arose from the selected voxel threshold and the cluster-based multiple correction method used. See also mean change across lifespan in Supporting Information Movies 1, 2 and 3 (contrast maps). To note, all significant effects showed negative rates of change; that is, all regions displayed decrements of contrast or signal intensity in Tp2 compared to Tp1.
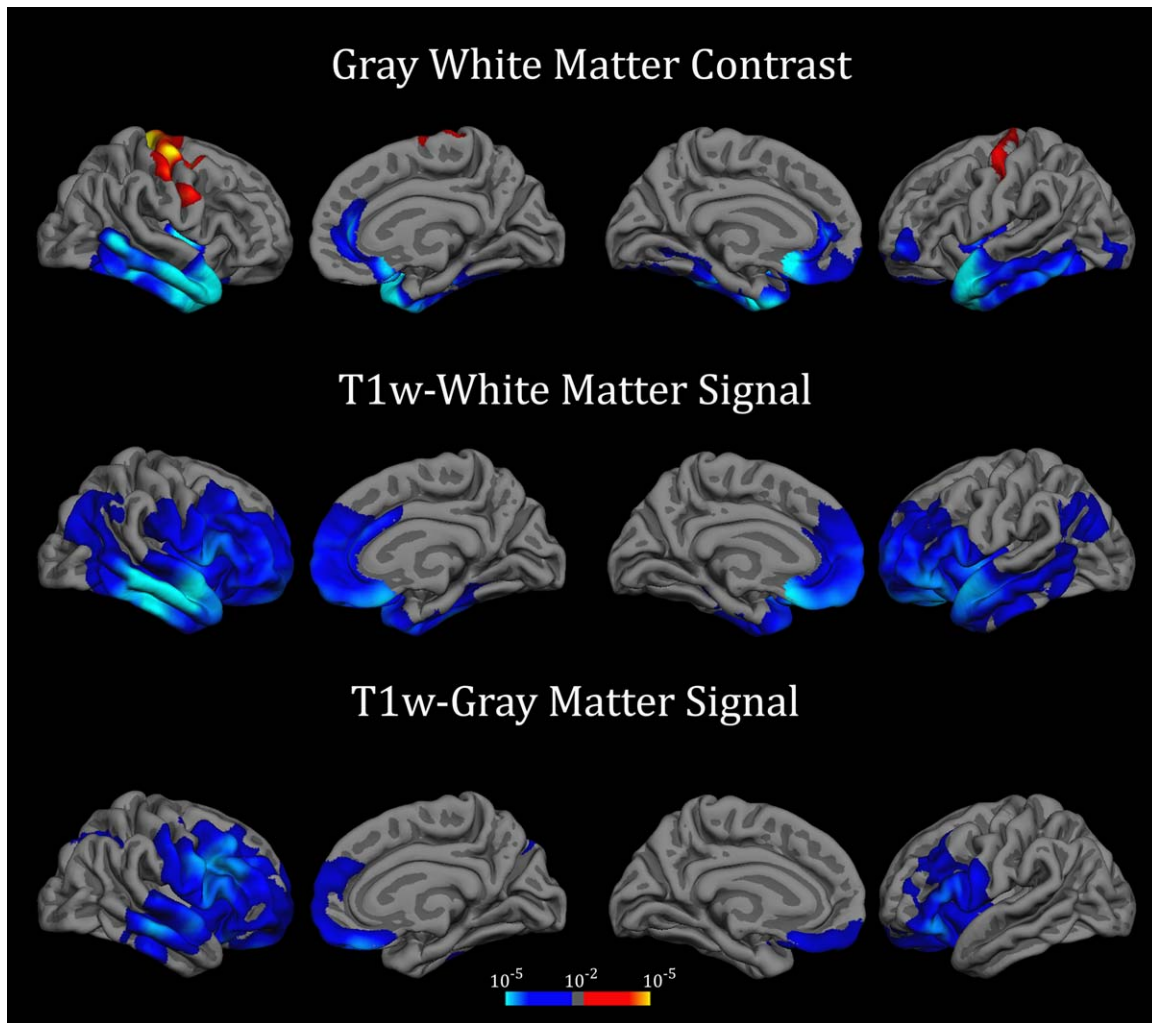
Figure 2.
Relationship between age and annual rates of change. Relationship between age and annual rate of GWC and signal intensity change after FWE correction for multiple comparisons. Results were thresholded at $P < 0.01$ vertex-wise and $P < 0.05$ cluster-based (Bonferroni corrected). Blue-Lightblue and Red-Yellow scales indicate acceleration and deceleration respectively of annual decline with advancing age (in P-values).

Relationship between GWC And T1w-Tissue Signal Intensity with Age over the Cortical Mantle

Age was related to GWC change in several brain areas; see maps displayed onto semi-inflated surfaces in Figure 2 and mean change across lifespan in Supporting Information Movies 1, 2 and 3 (contrast maps). Specifically, rate of GWC decline increased with age in the middle and anterior parts of the temporal lobes bilaterally, including the entorhinal cortices, the parahippocampal cortices, the temporal poles and the inferior and middle temporal gyri, as well as in the medial prefrontal cortex including the rostral anterior cingulate cortex and the medial orbitofrontal cortex. Associations between age and reduced decline were observed in somatosensory areas bilaterally. Age was also related to accelerated T1w signal decay in the WM, especially in dorsolateral prefrontal areas and in the medial prefrontal cortex including the rostral anterior cingulate cortex. A similar pattern was also found in the middle and anterior temporal lobe as well as in the left inferior parietal cortex bilaterally. Age was associated with T1w signal decrease in the GM in bilateral dorsolateral and medial prefrontal cortices as well as in the left middle temporal lobe.

GAMM Analysis and Spaghetti Plots of GWC And T1w-Tissue Across LifeSpan

Lifespan trajectories of GWC and signal intensity were additionally fitted with GAMM to more accurately delineate the age-trajectories and these are presented as spaghetti plots in Figure 3. As expected from previous vertex-wise analyses all ROIs but cuneus showed contrast blurring with age. Postcentral GWC seemed to decay in young participants and stabilize with advancing age, while rostral anterior cingulate and temporal lobes showed a relative stability of GWC followed by a pronounced decline in older participants with turning points in the seventh decade of life. The other frontal and parietal selected ROIs showed a stable decline of GWC across life. T1w signal intensity lifespan trajectories did not differ much between tissue classes, though the profiles were generally more pronounced when sampled in the subjacent WM. Temporal, pars triangularis and rostral anterior cingulate ROIs showed mild decline of signal intensity during early adulthood followed by a more pronounced decline in the seventh decade of life. Superior frontal and postcentral ROIs trajectories were relatively stable through the age-range while cuneus and supramarginal ROIs showed mild constant decrements of signal intensity during the adulthood.

Anatomical Comparison Between Myelin Maps and GWC, T1w-Tissue Decline in the Cortical Mantle

Anatomical differences in rate of GWC decline were unrelated to intracortical myelin content as indexed by T1w/T2w contrast maps obtained at baseline. Interestingly, anatomical maps of age effects on GWC and T1w-WM change showed high anatomical correspondence with intracortical myelin maps in both hemispheres. That is, accelerated decline of GWC and T1w-WM signal with age

were especially exacerbated in lightly myelinated areas. The correlation between myelin maps and interaction effects of GWC and T1w-WM change with age was high for both hemispheres (mean correlations across hemispheres $r \approx 0.69$ and $r \approx 0.57$ respectively). See full stats in Table II. Selected boxplots representing the median anatomical correlation of myelin content maps with change and age effects on change are shown in Figure 4. No correlation of any result estimates with myelin maps was found when mapped 1.0 mm into WM from GM/WM boundary. No significant differences in these results were found when the size of the subset was modified (data not shown).

Annual Change of GWC and T1w Signal Intensity and Age Interactions Across Cortical Parcellations and the Effect of Different Sampling Projections

Effects were in agreement with vertex-wise results when GWC and T1w signal intensity were analysed across cortical parcellations (Supporting Information Fig. 3). All the results were consistent across different sampling distances of signal intensity from the GM/WM boundary (see Supporting Information Figs. 4 and 5 for T1w intensities in the GM sampled at relative and fixed distances respectively).

DISCUSSION

Longitudinal GWC decline was found widespread over the cortical mantle, especially in the frontal lobes, with acceleration of decline with increased age in the temporal lobe and the medial prefrontal cortex. T1w signal intensity also declined longitudinally in the superficial WM across the cortex, as well as in the GM, though to a lesser degree, with accelerated decline with age in temporal and frontal

TABLE II. Anatomical correlation between baseline myelin content and estimates of GWC and T1w intensity change

| | | T1w/T2w myelin maps | | | | | |
| | | GM 0.2 mm distance | | GM 0.5 fraction | | WM 1.0 mm distance | |
		lh	rh	lh	rh	lh	rh
Rate	**GWC**	0.04	0.16	0.11	0.20	0.10	0.18
	T1w-WM	−0.34	0.10	−0.32	0.10	−0.08	0.00
	T1w-GM	−0.33	0.02	−0.35	0.00	−0.06	−0.05
Age*Rate	**GWC**	**0.73**	**0.73**	**0.67**	**0.63**	−0.17	0.23
	T1w-WM	**0.57**	**0.41**	**0.72**	**0.57**	−0.25	−0.32
	T1w-GM	−0.02	−0.25	0.09	−0.22	−0.08	−0.03

Values represent the median rank-based points for each hemisphere from the subsampling anatomical correlations between rate and rate*age estimates on one side and myelin content maps on the other. Median estimates-myelin anatomical correlations $r > 0.4$ are displayed in bold format. The arbitrary threshold of $r = 0.4$ corresponds to a moderate relationship [Cohen, 1988]. See Figure 4 for more information.
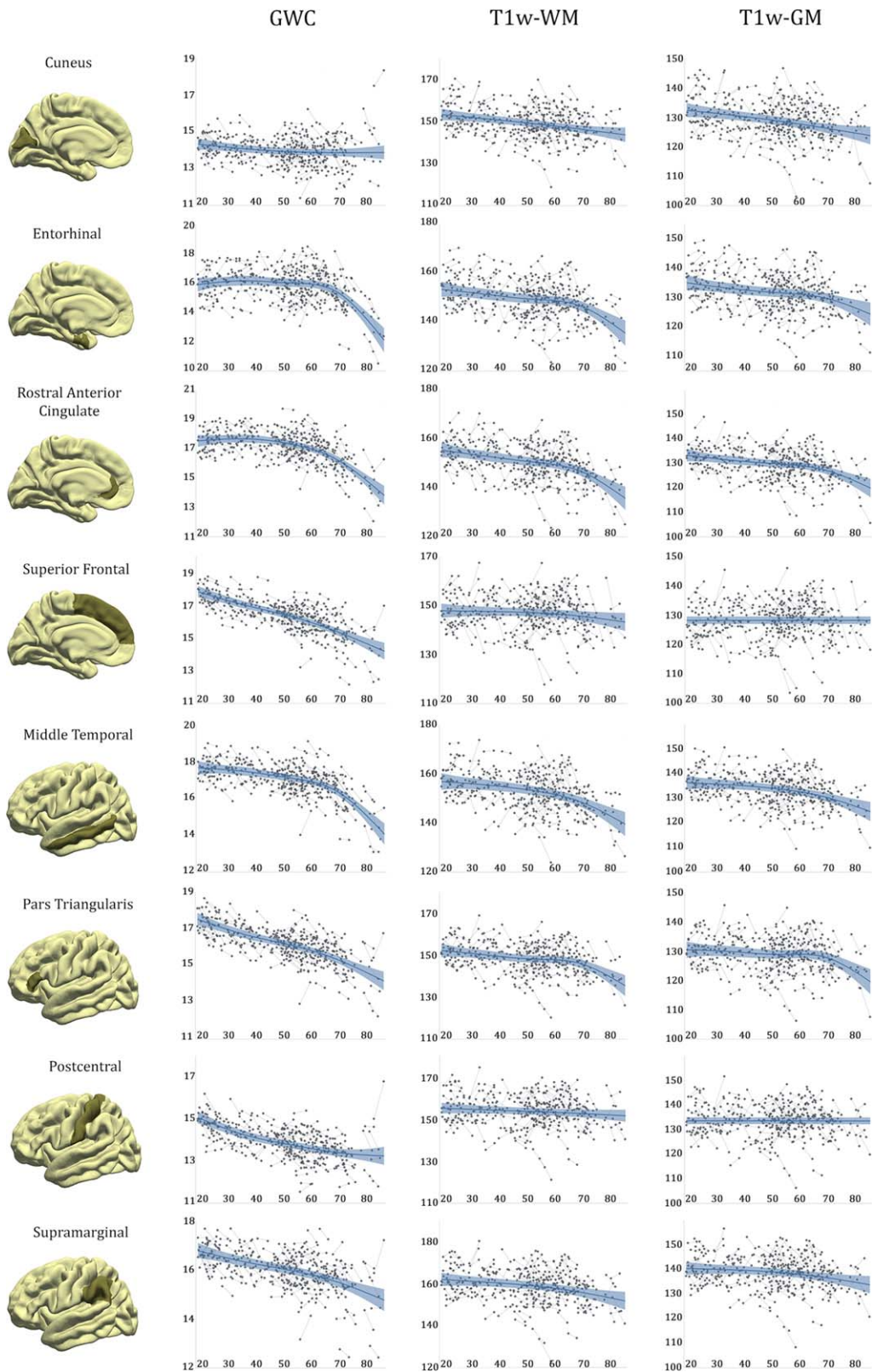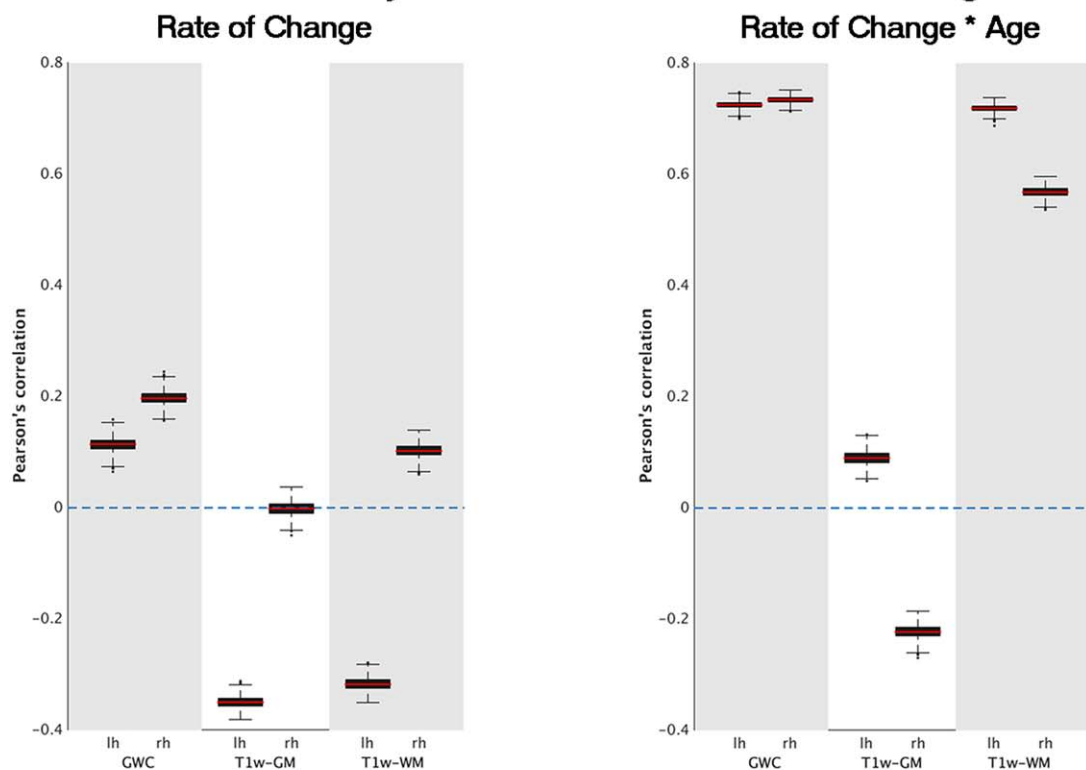
Figure 3.
Spaghetti plots of contrast and signal intensity. Spaghetti plots of contrast and signal intensity for representative bilateral regions as a function of age. For each region, the blue line represents the GAMM fitting while the lighter blue area corresponds to its confidence interval.
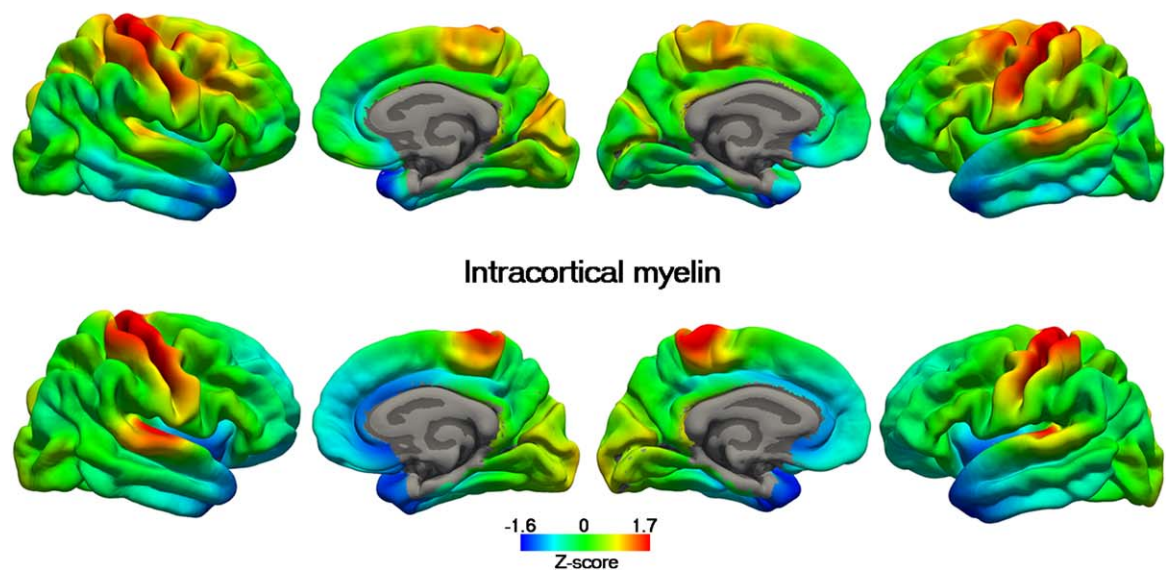
Figure 4.

Anatomical relationship between cortical myelin and accelerated GWC decline. In the upper part, boxplots representing the correlation between T1w/T2w myelin content maps sampled at mid-thickness (fraction = 0.5) and rate and rate*age estimates for GWC and T1w signal intensities. The red line represents the correlation between myelin and GWC and signal change estimates assessed as the median of n = 5000 correlations carried out with randomly selected subsamples of vertices. The black boxes represent the 25th and 75th percentile from all the random subsample correlations while whiskers denote correlations (with subsamples of vertices) with values deviating > 2 SD from the median (of the n = 5000 tests). In the lower side, z-normalized estimates of GWC and myelin content maps are displayed in a colour palette. Red represents more cortical myelin and deceleration of GWC decline with age while Lightblue represents lightly myelinated areas and accelerated decline with age respectively. See Table II for significant stats.

lobe areas. Importantly, acceleration of GWC decline with age was found mainly in thinly myelinated areas, supporting the theory of these regions being more vulnerable to detrimental effects of age [Bartzokis et al., 2001]. The implications of the results are discussed below.

Longitudinal GWC Contrast Decline

This study shows that longitudinal GWC changes can be detected in a healthy population over a relatively short period of time. Previously, Davatzikos and Resnick [2002] found decreased GWC signal in cognitively healthy older adults in several posterior, frontal and temporal areas using a voxel-based approach and a global GM measure. Grydeland and colleagues [2013a], however, only found increased GWC in a small posterior brain region in cognitively healthy older adults after a shorter interscan interval (≈ 2 years) while Alzheimer's Disease patients underwent GWC decrements in widespread areas of the prefrontal and temporal cortices, suggesting that GWC might be useful to distinguish between healthy and cognitively impaired populations [Grydeland et al., 2013b; Jefferson et al., 2014]. Importantly, the presently observed topological pattern of longitudinal GWC decrements in the superior and the inferior frontal cortices is highly consistent with the previous few reports that studied age-related trajectories of GWC cross-sectionally [Salat et al., 2009; Vidal-Piñeiro et al., 2014; Westlye et al., 2009].

An advantage of longitudinal studies is improved possibility to accurately delineate lifespan trajectories [Fjell et al., 2009a]. By this method, we delineated several patterns of GWC across adult lifespan, previously reported monotonic decreases of GWC in frontal and parietal areas and relative stability of GWC in the primary sensory areas across adulthood being two of them. The somatosensory cortex showed increases of GWC in the late older adulthood, but these results need to be taken with caution as GM/WM boundary delineation might be problematic in these areas [Glasser et al., 2013]. More interestingly, we found an acceleration of GWC decline with increasing age in the medial prefrontal cortex and in most of the temporal regions, including entorhinal and parahippocampal cortices. The pattern of accelerated decrements was found also in the T1w signal intensity especially when sampled in the superficial WM. Most of these areas are known to be especially sensitive to the detrimental effects of age over the brain; entorhinal acceleration of contrast decay matches evidence of increased cortical thinning with aging in the same area [Fjell et al., 2014b]. Also the other temporal areas, as well as the medial prefrontal cortex showed notable decrements of structural integrity (i.e. cortical thickness; [Fjell et al., 2009b; Fjell et al., 2013] and functional integrity (i.e. resting-state functional MRI connectivity; [Andrews-Hanna et al., 2007] with age, though controversies regarding the effects of age on the structural integrity of rostral anterior cingulate cortex [Gefen et al.,

2015]. Cortical signal decline, milder than GWC and T1-WM decline, was evident in posterior parietal and occipital regions while areas with acceleration of decline with age were mostly located in the prefrontal and temporal cortices. The present results are in agreement with a previous cross-sectional study [Westlye et al., 2010] that found increased T1w-GM signal decline in posterior areas with advancing age while frontal and temporal areas exhibited chronologically later peaks for maximal signal intensity and more accentuated quadratic trajectories during the entire lifespan. These results might relate to specific patterns of cortical myelination and to posterior to anterior shifts with aging [Davis et al., 2008] but do not easily fit with the lifespan trajectories of CTh nor with frontal aging hypotheses.

Caution is needed when interpreting the present results as neurobiological foundations of GWC and T1w intensity are not completely understood. Candidate mechanisms of signal intensity change are variations in structure and density of axonal myelin [Clark et al., 1991; Koenig, 1991; Walters et al., 2003], iron deposition [Ogg and Steen, 1998] and water content [Bansal et al., 2013], or most likely a combination of them [Eickhoff et al., 2005] as these biological candidates are often co-localized [Fukunaga et al., 2010; Sandell and Peters, 2003]. It has been proposed that T1w signal intensity alterations are driven by bioaccumulated iron [Ogg and Steen, 1998; Paus et al., 1999] which can also contribute to myelin susceptibility [Bartzokis et al., 2004]. While the influence of iron deposition on GWC lifespan trajectories cannot be discarded, cortical and subcortical T1w signal intensity lifespan trajectories were not strongly affected when controlled by T2* relaxation rates (secondary to iron depositions) [Westlye et al., 2010]. Quantitative MRI measures such as 1/T1 relaxation rates, that directly arise from biophysical properties of the sampled tissue and is correlated with T1w signal intensity, are increased in highly myelinated areas [Sereno et al., 2013; Sigalovsky et al., 2006] and reduced in aging [Agartz et al., 1991; Cho et al., 1997] in a region-specific fashion [Callaghan et al., 2014; Draganski et al., 2011]. Consistently high degree of myelinisation assessed ex-vivo corresponds to stronger T1w signal (Clark et al., 1990; Eickhoff et al., 2005; Walters et al., 2003). Despite strong contribution from myelin, T1w intensity results from a weighted sum of various cellular, neuroglial and other brain properties that can vary across cortical depths [Eickhoff et al., 2005]. Myelin-related changes in aged monkeys have been reported (reviewed in Peters, 2009, 2002), including fluid-filled balloons in the myelin sheaths, formations of redundant myelin and paranodes, splitting of the myelin lamellae and loss of myelinated fibers. Myelin changes seem to have an important role in volume and GM-WM volume ratio changes with aging [Courchesne et al., 2000; Courchesne and Plante, 1997]. As age-related decline in the GWC seems to be primarily driven by T1w-WM signal intensity reductions, the most prominent biological candidate

influencing the contrast is the degree of myelin in the superficial WM under the cortical mantle [Salat et al., 2009; Westlye et al., 2009].

Indeed, our adult lifespan trajectories are reminiscent to the age-related patterns found with T1w/T2w myelin content. In [Grydeland et al., 2013a], we characterized lifespan profiles of intracortical myelin together with myelin below cortical surface in a cross-sectional sample encompassing the entire lifespan. We showed intracortical myelin maturation until the late 30s and stabilization until the late 50s when losses of myelin were evident widespread the cortical surface. Interestingly, T1w/T2w contrast sampled in the superficial WM showed earlier stabilization of myelin content during development and a more pronounced decline in the old adults Also, adult T1w/T2w contrast lifespan trajectories showed a similar anatomical distribution to GWC, with pronounced loss of myelin in frontal, temporal and parietal regions, relatively stable myelin content during the whole adult lifespan in primary sensory areas and a more protracted and steep decline in the old adulthood in the temporal lobes. Also, GWC profile might be somewhat comparable to other recent studies focused on superficial WM through diffusion-based MRI techniques [Nazeri et al., 2015; Phillips et al., 2013]. Age-related superficial WM patterns showed strong decrements of WM integrity in regions such as rostral anterior cingulate and temporal cortices [Nazeri et al., 2015]. Heritability likely explains a significant amount of variation of GWC change [Panizzon et al., 2012], yet longitudinal evidence is still absent. Another reasonable contributor to variation of GWC with advancing age are cardiovascular risk factors [Jacobs et al., 2013]. It is also feasible that lifestyle variables, that can be introduced to the population, such as physical activity [Arnardottir et al., 2016], cognition training [Engvig et al., 2012] or nutrition habits [Witte et al., 2014] may modulate the GWC. However the factors that explain individual variability of GWC decline with advancing age still remain speculative.

Relationship Between Myelin Content and Age-Related GWC Decline

We found that accelerated GWC decline in aging was more prominent in lightly myelinated intracortical areas. This result was paralleled by T1w-WM signal lifespan trajectories but not by signal intensity patterns when sampled in the GM. Primary and early association cortices are heavily myelinated while higher multimodal cortices tend to be lightly myelinated, amongst them the temporal poles and the medial prefrontal cortices [Glasser and Van Essen, 2011; Nieuwenhuys, 2013]. More intracortical myelin content is associated with simpler and less dynamic circuits, probably by stabilizing circuitry and inhibiting plasticity to a certain extent [Glasser et al., 2014], while regions with high plasticity seems more vulnerable to detrimental effects of aging [Fjell et al., 2014a; Mesulam, 1999; Neill,

1995; Raz et al., 1997; Raz and Rodrigue, 2006]. Relationship of myelin maps fitted well with contrast decline acceleration maps supporting the idea of increased age-related vulnerability in highly plastic, lowly myelinated cortical areas. Thinly myelinated regions also tend to be late-myelinated areas, repeatedly reported to be more vulnerable to age-related neurodegeneration [Bartzokis et al., 2004; Raz, 2000; Reisberg et al., 1999]. Post-mortem studies with human and non-human primate brains show greater proportion of small-diameter fibers in the prefrontal and the temporal lobes while motor cortices and other primary sensory areas exhibit more large-diameter axonal fibers [Aboitiz et al., 1992; Caminiti et al., 2013; Liewald et al., 2014; Riise and Pakkenberg, 2011]. Not only is axonal diameter tied to degree of myelination [Riise and Pakkenberg, 2011], but small fibers seems particularly prone to age-related breakdown [Hou and Pakkenberg, 2012; Marner et al., 2003]. Likewise, such variation of size is closely tied to function, as small diameter fiber regions pack more densely allowing to carry more diverse information across processing areas [Aboitiz et al., 1992]. Of note, a relationship between myelin content and acceleration of T1w signal intensity change was evident when sampled into the WM but not intracortically in agreement with T1w-WM being the main measure of the contrast. Altogether GWC seems especially sensitive to age-related myelin variations underlying the GM/WM boundary of lightly myelinated areas. Thus GWC might arise as a useful technique to track myelin breakdown in critical brain regions both in normal aging and in clinical populations [Grydeland et al., 2013b; Jefferson et al., 2014; Salat et al., 2011; Westlye et al., 2009].

Limitations

The main limitations of the study are inherent to the measures employed, which do not allow a simple neurobiological interpretation of the results. One of the advantages of GWC, however, is that MRI scanner artefacts and field biases are minimized as nuisance signal from a given voxel is controlled by signal from adjacent voxels. The contrast is statistically more powerful to assess longitudinal differences and detect lifespan trajectories and have more topological variance than T1w signal intensity, probably due to controlled nuisance factors. However, T1w-GM signal also contains neurobiological information such as intracortical myelin content which varies across regions and declines with age [Agartz et al., 1991; Salat et al., 2009; Westlye et al., 2009, 2010]. While we outlined different lines of evidence favouring an interpretation of contrast blurring through lifespan as myelin breakdown in the superficial WM, intracortical myelin losses, captured with T1w-GM, might obscure GWC interpretation and its impact has to be taken into account, especially when no contrast decline is found. As an example, GWC lifespan stability in early processing cortical visual areas might be

due to losses of T1w-GM signal intensity that could be partially reflecting myelin decline in the outer line of Braillarger [Lintl and Braak, 1983] instead of lack of T1w-WM decline. While we showed that GWC profiles resemble those of T1w-WM and linked them to myeloarchitectonics, additional delineation of T1w signal intensity maps might facilitate GWC interpretation. Any technical contribution such as surface delineation that might affect GWC values also needs to be considered as it can bias contrast changes. However this concern is greatly reduced as: 1) the surface delineation was re-run from unbiased within-subject templates which minimizes reconstruction errors [Reuter et al., 2012]; 2) CTh, that would partially control longitudinal variations in surface delineation, was included as a covariate in all the analyses. CTh atrophy seems statistically independent of rate of GWC decline (Supporting Information Tables II and IV) as previously shown in cross-sectional studies [Salat et al., 2009; Westlye et al., 2009] and; 3) the results were robust to the sampling projection method used (Supporting Information Figs. 4 and 5). Another technical concern regards to the spatial resolution of the T1w images. While surface-based mapping allows for morphometric inferences on a sub-millimeter scale the mapped intensity values are still dependent on the native resolution of the image thus partial volume effects or errors in GM/WM boundary delineation are possible.

CONCLUSIONS

We found longitudinal changes in GWC contrast in widespread areas of the cortical mantle consistent with previous cross-sectional reports, probably related to myelin integrity changes in the superficial WM. GWC change was especially prominent in frontal areas and showed accelerated decline in medial prefrontal and temporal cortices. Accelerated decline in aging closely followed anatomical patterns of intracortical myelin content, supporting the theory of lightly myelinated regions being more vulnerable than highly-myelinated, more hard-wired regions such as the visual cortex. Thus, GWC assessed longitudinally might be a useful index to use alone or in combination to track the age-related changes in superficial myelin. Future GWC studies are needed to give further insight of its neurobiological substrates and link longitudinal contrast decline with cognitive and behavioural variation.

REFERENCES

Aboitiz F, Scheibel AB, Fisher RS, Zaidel E (1992): Fiber composition of the human corpus callosum. Brain Res 598:143–153.

Agartz I, Sääf J, Wahlund LO, Wetterberg L (1991): T1 and T2 relaxation time estimates in the normal human brain. Radiology 181:537–543.

Andrews-Hanna JR, Snyder AZ, Vincent JL, Lustig C, Head D, Raichle ME, Buckner RL (2007): Disruption of large-scale brain systems in advanced aging. Neuron 56:924–935.

Arnardottir NY, Koster A, Domelen DRV, Brychta RJ, Caserotti P, Eiriksdottir G, Sverrisdottir JE, Sigurdsson S, Johannsson E, Chen KY, Gudnason V, Harris TB, Launer LJ, Sveinsson T (2016): Association of change in brain structure to objectively measured physical activity and sedentary behavior in older adults: Age, Gene/Environment Susceptibility-Reykjavik Study. Behav Brain Res 296:118–124.

Bansal R, Hao X, Liu F, Xu D, Liu J, Peterson BS (2013): The effects of changing water content, relaxation times, and tissue contrast on tissue segmentation and measures of cortical anatomy in MR images. Magn Reson Imaging 31:1709–1730.

Bartsch H, Thompson WK, Jernigan TL, Dale AM (2014): A web-portal for interactive data exploration, visualization, and hypothesis testing. Front Neuroinformatics 8:25.

Bartzokis G, Beckson M, Lu PH, Nuechterlein KH, Edwards N, Mintz J (2001): Age-related changes in frontal and temporal lobe volumes in men: A magnetic resonance imaging study. Arch Gen Psychiatry 58:461–465.

Bartzokis G, Sultzer D, Lu PH, Nuechterlein KH, Mintz J, Cummings JL (2004): Heterogeneous age-related breakdown of white matter structural integrity: Implications for cortical "disconnection" in aging and Alzheimer's disease. Neurobiol Aging 25:843–851.

Beaulieu C (2002): The basis of anisotropic water diffusion in the nervous system—A technical review. NMR Biomed 15:435–455.

Beck, AT SR (1987): Beck Depression Inventory Scoring Manual Psychology. New York: Psychological.

Benes FM, Turtle M, Khan Y, Farol P (1994): Myelination of a key relay zone in the hippocampal formation occurs in the human brain during childhood, adolescence, and adulthood. Arch Gen Psychiatry 51:477–484.

Callaghan MF, Freund P, Draganski B, Anderson E, Cappelletti M, Chowdhury R, Diedrichsen J, Fitzgerald THB, Smittenaar P, Helms G, Lutti A, Weiskopf N (2014): Widespread age-related differences in the human brain microstructure revealed by quantitative magnetic resonance imaging. Neurobiol Aging 35:1862–1872.

Caminiti R, Carducci F, Piervincenzi C, Battaglia-Mayer A, Confalone G, Visco-Comandini F, Pantano P, Innocenti GM (2013): Diameter, length, speed, and conduction delay of callosal axons in macaque monkeys and humans: Comparing data from histology and magnetic resonance imaging diffusion tractography. J Neurosci off J Soc Neurosci 33:14501–14511.

Cho S, Jones D, Reddick WE, Ogg RJ, Steen RG (1997): Establishing norms for age-related changes in proton T1 of human brain tissue in vivo. Magn Reson Imaging 15:1133–1143.

Clark VP, Courchesne E, Grafe M (1991): In vivo myeloarchitectonic analysis of human striate and extrastriate cortex using magnetic resonance imaging. Cereb Cortex N Y N 2:417–424.

Cohen, J (1988): Statistical Power Analysis for the Behavioral Sciences, 2 edition. ed. Routledge, Hillsdale, N.J. USA.

Courchesne E, Plante E (1997): Measurement and analysis issues in neurodevelopmental magnetic resonance imaging. In: Developmental Neuroimaging: Mapping the Development of Brain and Behavior. Academic Press, San Diego, CA, USA. pp 43–65.

Courchesne E, Chisum HJ, Townsend J, Cowles A, Covington J, Egaas B, Harwood M, Hinds S, Press GA (2000): Normal brain development and aging: Quantitative analysis at in vivo MR imaging in healthy volunteers. Radiology 216:672–682.

Dale AM, Fischl B, Sereno MI (1999): Cortical surface-based analysis. I. Segmentation and surface reconstruction. NeuroImage 9:179–194.

Davatzikos C, Resnick SM (2002): Degenerative age changes in white matter connectivity visualized in vivo using magnetic resonance imaging. Cereb Cortex N Y N 12:767–771. 1991

Davis SW, Dennis NA, Daselaar SM, Fleck MS, Cabeza R (2008): Que PASA? The posterior-anterior shift in aging. Cereb Cortex N Y N 18:1201–1209. 1991

Delis D, Kramer J, Kaplan E, Ober B (2000): California verbal learning test (CVLT-II), 2nd ed. San Antonio, TX: Psychological.

Desikan RS, Ségonne F, Fischl B, Quinn BT, Dickerson BC, Blacker D, Buckner RL, Dale AM, Maguire RP, Hyman BT, Albert MS, Killiany RJ (2006): An automated labeling system for subdividing the human cerebral cortex on MRI scans into gyral based regions of interest. NeuroImage 31:968–980.

Draganski B, Ashburner J, Hutton C, Kherif F, Frackowiak RSJ, Helms G, Weiskopf N (2011): Regional specificity of MRI contrast parameter changes in normal ageing revealed by voxel-based quantification (VBQ). NeuroImage 55:1423–1434.

Eickhoff S, Walters NB, Schleicher A, Kril J, Egan GF, Zilles K, Watson JDG, Amunts K (2005): High-resolution MRI reflects myeloarchitecture and cytoarchitecture of human cerebral cortex. Hum Brain Mapp 24:206–215.

Engvig A, Fjell AM, Westlye LT, Moberget T, Sundseth Ø, Larsen VA, Walhovd KB (2012): Memory training impacts short-term changes in aging white matter: A longitudinal diffusion tensor imaging study. Hum Brain Mapp 33:2390–2406.

Feldman ML, Peters A (1998): Ballooning of myelin sheaths in normally aged macaques. J Neurocytol 27:605–614.

Fischl B, Dale AM (2000): Measuring the thickness of the human cerebral cortex from magnetic resonance images. Proc Natl Acad Sci U S A 97:11050–11055.

Fischl B, Sereno MI, Dale AM (1999a): Cortical surface-based analysis. II: Inflation, flattening, and a surface-based coordinate system. NeuroImage 9:195–207.

Fischl B, Sereno MI, Tootell RB, Dale AM (1999b): High-resolution intersubject averaging and a coordinate system for the cortical surface. Hum Brain Mapp 8:272–284.

Fischl B, Salat DH, Busa E, Albert M, Dieterich M, Haselgrove C, van der Kouwe A, Killiany R, Kennedy D, Klaveness S, Montillo A, Makris N, Rosen B, Dale AM (2002): Whole brain segmentation: Automated labeling of neuroanatomical structures in the human brain. Neuron 33:341–355.

Fischl B, van der Kouwe A, Destrieux C, Halgren E, Ségonne F, Salat DH, Busa E, Seidman LJ, Goldstein J, Kennedy D, Caviness V, Makris N, Rosen B, Dale AM (2004a): Automatically parcellating the human cerebral cortex. Cereb Cortex N Y N 1991 14:11–22.

Fischl B, Salat DH, van der Kouwe AJW, Makris N, Ségonne F, Quinn BT, Dale AM (2004b): Sequence-independent segmentation of magnetic resonance images. NeuroImage 23 Suppl 1: S69–S84.

Fjell AM, Westlye LT, Greve DN, Fischl B, Benner T, van der Kouwe AJW, Salat D, Bjørnerud A, Due-Tønnessen P, Walhovd KB (2008): The relationship between diffusion tensor imaging and volumetry as measures of white matter properties. NeuroImage 42:1654–1668.

Fjell AM, Walhovd KB, Fennema-Notestine C, McEvoy LK, Hagler DJ, Holland D, Brewer JB, Dale AM (2009a): One-year brain atrophy evident in healthy aging. J Neurosci off J Soc Neurosci 29:15223–15231.

Fjell AM, Westlye LT, Amlien I, Espeseth T, Reinvang I, Raz N, Agartz I, Salat DH, Greve DN, Fischl B, Dale AM, Walhovd KB (2009b): High consistency of regional cortical thinning in aging across multiple samples. Cereb Cortex N Y N 1991 19: 2001–2012.

Fjell AM, McEvoy L, Holland D, Dale AM, Walhovd KB, Alzheimer's Disease Neuroimaging Initiative (2013): Brain changes in older adults at very low risk for Alzheimer's disease. J Neurosci off J Soc Neurosci 33:8237–8242.

Fjell AM, McEvoy L, Holland D, Dale AM, Walhovd KB, Alzheimer's Disease Neuroimaging Initiative (2014a): What is normal in normal aging? Effects of aging, amyloid and Alzheimer's disease on the cerebral cortex and the hippocampus. Prog Neurobiol 117:20–40.

Fjell AM, Westlye LT, Grydeland H, Amlien I, Espeseth T, Reinvang I, Raz N, Dale AM, Walhovd KB (2014b): Accelerating cortical thinning: Unique to dementia or universal in aging? Cereb Cortex N Y N 1991 24:919–934.

Folstein MF, Folstein SE, McHugh PR (1975): "Mini-mental state". A practical method for grading the cognitive state of patients for the clinician. J Psychiatr Res 12:189–198.

Fukunaga M, Li T-Q, van Gelderen P, de Zwart JA, Shmueli K, Yao B, Lee J, Maric D, Aronova MA, Zhang G, Leapman RD, Schenck JF, Merkle H, Duyn JH (2010): Layer-specific variation of iron content in cerebral cortex as a source of MRI contrast. Proc Natl Acad Sci U S A 107:3834–3839.

Gefen T, Peterson M, Papastefan ST, Martersteck A, Whitney K, Rademaker A, Bigio EH, Weintraub S, Rogalski E, Mesulam M-M, Geula C (2015): Morphometric and histologic substrates of cingulate integrity in elders with exceptional memory capacity. J Neurosci 35:1781–1791.

Glasser MF, Van Essen DC (2011): Mapping human cortical areas in vivo based on myelin content as revealed by T1- and T2-weighted MRI. J Neurosci off J Soc Neurosci 31:11597–11616.

Glasser MF, Sotiropoulos SN, Wilson JA, Coalson TS, Fischl B, Andersson JL, Xu J, Jbabdi S, Webster M, Polimeni JR, Van Essen DC, Jenkinson M, WU-Minn HCP Consortium (2013): The minimal preprocessing pipelines for the Human Connectome Project. NeuroImage 80:105–124.

Glasser MF, Goyal MS, Preuss TM, Raichle ME, Van Essen DC (2014): Trends and properties of human cerebral cortex: Correlations with cortical myelin content. NeuroImage 93:165–175.

Greve DN, Fischl B (2009): Accurate and robust brain image alignment using boundary-based registration. NeuroImage 48: 63–72.

Grydeland H, Walhovd KB, Tamnes CK, Westlye LT, Fjell AM (2013a): Intracortical myelin links with performance variability across the human lifespan: Results from T1- and T2-weighted MRI myelin mapping and diffusion tensor imaging. J Neurosci off J Soc Neurosci 33:18618–18630.

Grydeland H, Westlye LT, Walhovd KB, Fjell AM (2013b): Improved prediction of Alzheimer's disease with longitudinal white matter/gray matter contrast changes. Hum Brain Mapp 34:2775–2785.

Hagler DJ, Saygin AP, Sereno MI (2006): Smoothing and cluster thresholding for cortical surface-based group analysis of fMRI data. NeuroImage 33:1093–1103.

Haroutunian V, Katsel P, Roussos P, Davis KL, Altshuler LL, Bartzokis G (2014): Myelination, oligodendrocytes, and serious mental illness. Glia 62:1856–1877.

Hayasaka S, Nichols TE (2003): Validating cluster size inference: Random field and permutation methods. NeuroImage 20:2343–2356.

Hou J, Pakkenberg B (2012): Age-related degeneration of corpus callosum in the 90+ years measured with stereology. Neurobiol Aging 33:1009.e1–1009.

Jacobs HIL, Leritz EC, Williams VJ, Van Boxtel MPJ, van der Elst W, Jolles J, Verhey FRJ, McGlinchey RE, Milberg WP, Salat DH (2013): Association between white matter microstructure, executive functions, and processing speed in older adults: The impact of vascular health. Hum Brain Mapp 34:77–95.

Jefferson AL, Gifford KA, Damon S, Chapman GW, Liu D, Sparling J, Dobromyslin V, Salat D (2015): Gray & white matter tissue contrast differentiates Mild Cognitive Impairment converters from non-converters. Brain Imaging Behav 9:141–148.

Jovicich J, Czanner S, Greve D, Haley E, van der Kouwe A, Gollub R, Kennedy D, Schmitt F, Brown G, Macfall J, Fischl B, Dale A (2006): Reliability in multi-site structural MRI studies: Effects of gradient non-linearity correction on phantom and human data. NeuroImage 30:436–443.

Koenig SH (1991): Cholesterol of myelin is the determinant of gray-white contrast in MRI of brain. Magn Reson Med off J Soc Magn Reson Med Soc Magn Reson Med 20:285–291.

Lakens D (2013): Calculating and reporting effect sizes to facilitate cumulative science: A practical primer for t-tests and ANOVAs. Front Psychol 4:863.

Liewald D, Miller R, Logothetis N, Wagner H-J, Schüz A (2014): Distribution of axon diameters in cortical white matter: An electron-microscopic study on three human brains and a macaque. Biol Cybern 108:541–557.

Lintl P, Braak H (1983): Loss of intracortical myelinated fibers: A distinctive age-related alteration in the human striate area. Acta Neuropathol (Berl) 61:178–182.

Magnaldi S, Ukmar M, Vasciaveo A, Longo R, Pozzi-Mucelli RS (1993): Contrast between white and grey matter: MRI appearance with ageing. Eur Radiol 3:

Marner L, Nyengaard JR, Tang Y, Pakkenberg B (2003): Marked loss of myelinated nerve fibers in the human brain with age. J Comp Neurol 462:144–152.

Mesulam MM (1999): Neuroplasticity failure in Alzheimer's disease: Bridging the gap between plaques and tangles. Neuron 24:521–529.

Miller DJ, Duka T, Stimpson CD, Schapiro SJ, Baze WB, McArthur MJ, Fobbs AJ, Sousa AMM, Sestan N, Wildman DE, Lipovich L, Kuzawa CW, Hof PR, Sherwood CC (2012): Prolonged myelination in human neocortical evolution. Proc Natl Acad Sci U S A 109:16480–16485.

Nazeri A, Chakravarty MM, Rajji TK, Felsky D, Rotenberg DJ, Mason M, Xu LN, Lobaugh NJ, Mulsant BH, Voineskos AN (2015): Superficial white matter as a novel substrate of age-related cognitive decline. Neurobiol Aging 36:2094–2106.

Neill D (1995): Alzheimer's disease: Maladaptive synaptoplasticity hypothesis. Neurodegener J Neurodegener Disord Neuroprotection Neuroregeneration 4:217–232.

Nieuwenhuys R (2013): The myeloarchitectonic studies on the human cerebral cortex of the Vogt-Vogt school, and their significance for the interpretation of functional neuroimaging data. Brain Struct Funct 218:303–352.

Ogg RJ, Steen RG (1998): Age-related changes in brain T1 are correlated with iron concentration. Magn Reson Med off J Soc Magn Reson Med Soc Magn Reson Med 40:749–753.

Panizzon MS, Fennema-Notestine C, Kubarych TS, Chen C-H, Eyler LT, Fischl B, Franz CE, Grant MD, Hamza S, Jak A, Jernigan TL, Lyons MJ, Neale MC, Prom-Wormley EC, Seidman L, Tsuang MT, Wu H, Xian H, Dale AM, Kremen WS (2012): Genetic and environmental influences of white and gray matter signal contrast: A new phenotype for imaging genetics? NeuroImage 60:1686–1695.

Paus T, Zijdenbos A, Worsley K, Collins DL, Blumenthal J, Giedd JN, Rapoport JL, Evans AC (1999): Structural maturation of neural pathways in children and adolescents: In vivo study. Science 283:1908–1911.

Peters A (2002): The effects of normal aging on myelin and nerve fibers: A review. J Neurocytol 31:581–593.

Peters A (2009): The effects of normal aging on myelinated nerve fibers in monkey central nervous system. Front Neuroanat 3:11.

Phillips OR, Clark KA, Luders E, Azhir R, Joshi SH, Woods RP, Mazziotta JC, Toga AW, Narr KL (2013): Superficial white matter: Effects of age, sex, and hemisphere. Brain Connect 3:146–159.

Raz N (2000): Aging of the brain and its impact on cognitive performance: Integration of structural and functional findings. In: Handbook of Aging and Cognition - II. NJ: Erlbaum. pp 1–90.

Raz N, Rodrigue KM (2006): Differential aging of the brain: Patterns, cognitive correlates and modifiers. Neurosci Biobehav Rev 30:730–748.

Raz N, Millman D, Sarpel G (1990): Cerebral correlates of cognitive aging: Gray-white-matter differentiation in the medial temporal lobes, and fluid versus crystallized abilities. Psychobiology 18:475–481.

Raz N, Gunning FM, Head D, Dupuis JH, McQuain J, Briggs SD, Loken WJ, Thornton AE, Acker JD (1997): Selective aging of the human cerebral cortex observed in vivo: Differential vulnerability of the prefrontal gray matter. Cereb Cortex 7:268–282.

Reisberg B, Franssen EH, Hasan SM, Monteiro I, Boksay I, Souren LE, Kenowsky S, Auer SR, Elahi S, Kluger A (1999): Retrogenesis: Clinical, physiologic, and pathologic mechanisms in brain aging, Alzheimer's and other dementing processes. Eur Arch Psychiatry Clin Neurosci 249 Suppl 3:28–36.

Reuter M, Schmansky NJ, Rosas HD, Fischl B (2012): Within-subject template estimation for unbiased longitudinal image analysis. NeuroImage 61:1402–1418.

Riise J, Pakkenberg B (2011): Stereological estimation of the total number of myelinated callosal fibers in human subjects. J Anat 218:277–284.

Salat DH, Lee SY, van der Kouwe AJ, Greve DN, Fischl B, Rosas HD (2009): Age-associated alterations in cortical gray and white matter signal intensity and gray to white matter contrast. NeuroImage 48:21–28.

Salat DH, Chen JJ, van der Kouwe AJ, Greve DN, Fischl B, Rosas HD (2011): Hippocampal degeneration is associated with temporal and limbic gray matter/white matter tissue contrast in Alzheimer's disease. NeuroImage 54:1795–1802.

Sandell JH, Peters A (2003): Disrupted myelin and axon loss in the anterior commissure of the aged rhesus monkey. J Comp Neurol 466:14–30.

Sereno MI, Lutti A, Weiskopf N, Dick F (2013): Mapping the human cortical surface by combining quantitative T(1) with retinotopy. Cereb Cortex N Y N 1991 23:2261–2268.

Shafee R, Buckner RL, Fischl B (2015): Gray matter myelination of 1555 human brains using partial volume corrected MRI images. NeuroImage 105:473–485.

Sigalovsky IS, Fischl B, Melcher JR (2006): Mapping an intrinsic MR property of gray matter in auditory cortex of living humans: A possible marker for primary cortex and hemispheric differences. NeuroImage 32:1524–1537.

Sled JG, Zijdenbos AP, Evans AC (1998): A nonparametric method for automatic correction of intensity nonuniformity in MRI data. IEEE Trans Med Imaging 17:87–97.

Song S-K, Yoshino J, Le TQ, Lin S-J, Sun S-W, Cross AH, Armstrong RC (2005): Demyelination increases radial diffusivity in corpus callosum of mouse brain. NeuroImage 26: 132–140.

Storsve AB, Fjell AM, Tamnes CK, Westlye LT, Overbye K, Aasland HW, Walhovd KB (2014): Differential longitudinal changes in cortical thickness, surface area and volume across the adult life span: Regions of accelerating and decelerating change. J Neurosci off J Soc Neurosci 34:8488–8498.

Vidal-Piñeiro D, Valls-Pedret C, Fernández-Cabello S, Arenaza-Urquijo EM, Sala-Llonch R, Solana E, Bargalló N, Junqué C, Ros E, Bartrés-Faz D (2014): Decreased Default Mode Network connectivity correlates with age-associated structural and cognitive changes. Front Aging Neurosci 6:256.

Walters NB, Egan GF, Kril JJ, Kean M, Waley P, Jenkinson M, Watson JDG (2003): In vivo identification of human cortical areas using high-resolution MRI: An approach to cerebral structure-function correlation. Proc Natl Acad Sci U S A 100: 2981–2986.

Wechsler D (1999): Wechsler Abbreviated Scale of Intelligence. San Antonio, TX: Psychological.

Westlye LT, Walhovd KB, Dale AM, Espeseth T, Reinvang I, Raz N, Agartz I, Greve DN, Fischl B, Fjell AM (2009): Increased sensitivity to effects of normal aging and Alzheimer's disease on cortical thickness by adjustment for local variability in gray/white contrast: A multi-sample MRI study. NeuroImage 47:1545–1557.

Westlye LT, Walhovd KB, Dale AM, Bjørnerud A, Due-Tønnessen P, Engvig A, Grydeland H, Tamnes CK, Østby Y, Fjell AM (2010): Differentiating maturational and aging-related changes of the cerebral cortex by use of thickness and signal intensity. NeuroImage 52:172–185.

Westlye LT, Grydeland H, Walhovd KB, Fjell AM (2011): Associations between regional cortical thickness and attentional networks as measured by the attention network test. Cereb Cortex N Y N 21:345–356. (1991):

Witte AV, Kerti L, Hermannstädter HM, Fiebach JB, Schreiber SJ, Schuchardt JP, Hahn A, Flöel A (2014): Long-chain omega-3 fatty acids improve brain function and structure in older adults. Cereb Cortex N Y N 1991 24:3059–3068.

Wood SN (2006): Generalized Additive Models: An Introduction With R. Boca Raton, Florida, U. S. A.: Chapman Hall/CRC. Available at: http://www.crcpress.com/product/isbn/9781584884743.

Yakovlev P, Lecours A (1967): The myelogenic cycles of regional maturation of the brain. In: Regional Development of the Brain in Early Life. Oxford and Edinburg: Blackwell Scientific Publications. pp 3–70.